Joint Centre for Mesoscale Meteorology, Reading, UK

A Parametrization Scheme for Symmetric Instability: Tests for an Idealised Flow

A. J. Thorpe
C. S. Chan

Internal Report No. 14

February 1993

Met Office **Joint** Centre for Mesoscale Meteorology Department of Meteorology
University of Reading PO Box 243 Reading RG6 6BB United Kingdom
Tel: +44 (0)118 931 8425 Fax: +44 (0)118 931 8791
www.metoffice.com

Designed and produced by the Met Office © Crown copyright 2001 01/0240 The Met Office logo is a registered trademark.

A Parametrization Scheme for Symmetric Instability: Tests for an Idealised Flow

Chou Sin Chan Alan J Thorpe

Department of Meteorology

University of Reading, England

Abstract

The existence of conditional symmetric instability (CSI) in the atmosphere has been established both in mid-latitude cyclones and in tropical cyclones. It leads to cloud bands oriented parallel to the thermal wind vector in a flow which exhibits either two-dimensional or circular symmetry. The result of the release of this instability is that the atmosphere approaches a state of neutrality in which the equivalent potential vorticity is near zero. In this paper a parametrization scheme is described which includes such cloud processes in the context of the mass flux formulation currently implemented at ECMWF. It is shown that, similar to convective clouds, the trajectory of an updraught (or downdraught) parcel is an important parameter which must be separately input to the scheme. For convective clouds this is always taken to be vertical whereas for CSI this typical trajectory follows a sloping path. Here we take this path to be along a line of neutral buoyancy intersecting the parcel initial lifting level location; this is justified by reference to linear and non-linear models of CSI. As a consequence an ascending parcel, in an unstable atmosphere, acquires an (absolute) momentum anomaly. The parcel undergoes entrainment and detrainment and effects a vertical mixing of momentum. The point is made that CSI cloud organisation is the only situation where such "cumulus friction" is dynamically justified. Results of applying the scheme to a single column and to a two-dimensional flow containing a local region of instability are presented. A representation of large-scale forcing of the instability is also included.

1 Introduction

Current convective parametrization schemes make no explicit allowance for the different organisation regimes clouds are known to fall into. As far as cloud dynamics is concerned there are distinct phenomena depending on the flow and thermodynamic structure in which the clouds develop. The following is probably not an exhaustive list:

convection: isolated storms - supercell
short-lived showers
shallow (boundary-layer) clouds
mid-level convection
squall lines - mid-latitude
tropical
multicellular storms - travelling
stationary
mesoscale convective complexes
conditional symmetric instability: frontal rainbands
axisymmetric bands in tropical cyclones

There are special schemes to account separately for mid-level convection and shallow boundary layer clouds but only in terms of their distinctive thermodynamic properties. To a cloud dynamicist it seems surprising that separate account is not taken for all of the above cloud organisation types. No where is this lack of discrimination more acute than when it comes to the question of the momentum flux. But even the geometrical problem of the way in which a squall line, which may be $500km$ long by $50km$ wide, is different from a supercell, which may occupy an area of perhaps $50km$ by $50km$, seems not to have been faced. The reasons are to do with the hypothesis that sub-grid-scale clouds need to be statistically many for their overall effects to be representable. It is clear that most deep clouds occur in an organised fashion often well isolated from nearest neighbours.

Clearly the issue of mesoscale organisation is an extremely difficult one involving questions such as the scale separation of the clouds from the model grid spacing. It is the contention here that cloud bands which are essentially two-dimensional, such as frontal

rain or snow bands and squall lines, offer the most important challenge to conventional parametrization schemes. A further crucial difficulty for current schemes is that these phenomena can exist in a quasi (or statistical) steady state for many hours and can, in that time, propagate over many grid squares. Here we consider in detail frontal rainbands which are due to conditional symmetric instability (CSI). These are particularly of interest as no operational forecast model as yet makes specific allowance for this instability. Is the space or time scale of these phenomena such that they need to be parametrized in current models? The growth rate of the instability might be a few hours whilst such bands may be present over the complete life of a front of, say, 1 to 3 days. The spatial scales are highly anisotropic with cross-frontal scales being in the range of 20 to $200km$ and along-front scales from 200 to $2000km$. So these phenomena are uncomfortably at the spatial resolution of current global weather forecast models; they will be substantially sub-grid scale for climate models for some time to come.

Nordeng 1987 included in an operational model with $50km$ horizontal resolution a Kuo-type parametrization of CSI. The precipitation from this parametrization could be found in bands and complemented that from vertical convection and large scale precipitation. Lindstrom and Nordeng 1992 showed that greater horizontal resolution can also affect the precipitation amount through stronger and narrower grid-scale updraughts. In Nordeng's scheme (in this issue) the neutrality to symmetric instability is achieved by adjusting the equivalent potential temperature along the absolute momentum surfaces. Parcels of air are displaced along absolute momentum surfaces, the buoyancy is checked, and a modified Kuo scheme is applied on the temperature and moisture fields.

The formulation we will develop here is perhaps unique in cloud parametrization schemes in that we deliberately set out to confront, and answer, the problem of cloud momentum fluxes. We use the current ECMWF formulation for convection with the mass flux scheme but modify it to cope with CSI. To illustrate the scheme we will use a dry analogy although the essential physics is not substantially different in concept for the full moist case. In the full implementation there will, in addition to the momentum fluxes described here, be latent heating due to condensation as parcels ascend along moist isentropic surfaces. For the background to CSI the reader is referred to the following papers: basic dynamics - Bennetts and Hoskins 1979, Emanuel 1983, Thorpe and Rotunno

1989 and Jones and Thorpe 1992; observational evidence - Emanuel 1988, Sanders and Bosart 1985, and Thorpe and Clough 1991. For the background to the mass flux scheme we follow Tiedtke 1989.

2 The Instability Criterion

There are many ways to describe the criterion for symmetric instability. The linear model shows that the potential vorticity (PV) must be negative which is equivalent for a geostrophic two-dimensional flow to a condition on the Richardson number. The linear model and non-linear simulations such as discussed in Thorpe and Rotunno 1989 show that the maximum growth rate is obtained for ascent close to the basic state isentropes depending on the degree that the motion satisfies the hydrostatic approximation. The parcel approach described by Emanuel 1983 quantifies the forces acting on a displaced parcel. Thorpe et al 1989 show that the neutral buoyancy displacement releases maximum parcel kinetic energy. For a parametrization scheme the parcel model is useful because the schemes are usually based on lifting a parcel to calculate whether instability is present. All such calculations, even for convection, require the path of the lifted parcel to be prescribed. Bearing in mind the above results on the likely parcel path we choose the neutral buoyancy trajectory. Results, not shown here, have been obtained for other assumed paths but the mathematical formulation to be given now makes the neutral buoyancy assumption.

The instability criterion for a parcel lifted in a two-dimensional flow in a direction $\mathbf{x}$ orthogonal to the thermal wind but along a neutral buoyancy curve is:

$$f\hat{m}\tilde{x} > 0 \tag{1}$$

where $\hat{m}$ is the difference between the parcel absolute momentum ($m = v_g + fx$) and that of its current surroundings, and $\tilde{x}$ is its x-displacement along a neutral buoyancy curve. The above criterion is general and applies to both hemispheres, either sign of baroclinity, and for ascending as well as descending parcels. For reference note that the criterion for convection arises from lifting a parcel vertically over a distance $\tilde{z}$:

$$g\hat{\theta}\tilde{z} > 0$$

where $\hat{\theta}$ is the parcel's anomaly of potential temperature (or more accurately density). The scheme to be tested here will operate whenever convective instability, as just defined, is not present. There has been recent speculation about the use of a CSI scheme to account for both CSI and convection. Whilst this is a possibility worth exploring the practical difficulties are not discussed here.

In Figure 1 a schematic of the disposition of θ and m surfaces is given and the assumed parcel path. In the example of Figure 1, taken from the northern hemisphere for a baroclinic flow with cold air lying to the west, the above general criterion reduces to $\hat{m} < 0$ as $\tilde{x}$ is less than zero. This hypothetical undilute ascending parcel achieves neutral buoyancy at the point marked T at which $\hat{m} = 0$. The existence of such momentum anomalies has been found in non-linear simulations, see Figure 2 of Thorpe and Rotunno 1989, and in frontal observations, see Thorpe and Clough 1991.

Here we deal with tests of the parametrization scheme in a two-dimensional flow in which $\frac{\partial}{\partial y} = 0$. In applying the scheme to an operational model a local coordinate system must be calculated oriented along and across the thermal wind direction. This and the consequent interpolation will require the solution of same practical implementation problems which are not faced here.

3 Mass Flux Scheme for CSI

Consider a dry atmosphere with a basic state in hydrostatic and geostrophic balance and frictionless. The large scale equations for heat and absolute momentum, $m = v_g + fx$, can be written as:

$$\frac{\partial \bar{\theta}}{\partial t} + \bar{\mathbf{v}}.\nabla\bar{\theta} + \bar{w}\frac{\partial \bar{\theta}}{\partial z} = -\frac{1}{\bar{\rho}}\nabla.\left(\bar{\rho}\overline{\mathbf{v}'\theta'}\right) - \frac{1}{\bar{\rho}}\frac{\partial(\bar{\rho}\overline{w'\theta'})}{\partial z} + \frac{\bar{Q}_R}{Cp} \tag{2}$$

$$\frac{\partial \bar{m}}{\partial t} + \bar{\mathbf{v}}.\nabla\bar{m} + \bar{w}\frac{\partial \bar{m}}{\partial z} = -\frac{1}{\bar{\rho}}\nabla.\left(\bar{\rho}\overline{\mathbf{v}'m'}\right) - \frac{1}{\bar{\rho}}\frac{\partial(\bar{\rho}\overline{w'm'})}{\partial z} \tag{3}$$

The '$-$' denotes average over a horizontal area which contains the ensemble of clouds. $\overline{\mathbf{v}'\theta'}$, $\overline{\mathbf{v}'m'}$, $\overline{w'\theta'}$ and $\overline{w'm'}$, are eddy transports of heat and momentum in the horizontal and vertical, respectively, and $\frac{\bar{Q}_R}{C_p}$ is the radiative heating. The flow has been assumed to

be two dimensional, i.e. $\frac{\partial}{\partial y} \approx 0$. The contributions to θ and m of the environment due to symmetric instability are:

$$\frac{\partial \bar{\theta}}{\partial t} = -\frac{1}{\bar{\rho}} \frac{\partial \left(\overline{\bar{\rho} u' \theta'}\right)_{SI}}{\partial x} - \frac{1}{\bar{\rho}} \frac{\partial \left(\overline{\bar{\rho} w' \theta'}\right)_{SI}}{\partial z} \tag{4}$$

$$\frac{\partial \bar{m}}{\partial t} = -\frac{1}{\bar{\rho}} \frac{\partial \left(\overline{\bar{\rho} u' m'}\right)_{SI}}{\partial x} - \frac{1}{\bar{\rho}} \frac{\partial \left(\overline{\bar{\rho} w' m'}\right)_{SI}}{\partial z} \tag{5}$$

The above expressions show that the adjustment towards a neutral state can be done through the distribution of heating and/or momentum in the atmosphere. Based on the linear theory, which shows the most unstable mode occurs in the direction parallel to the θ surfaces, a crucial assumption is made for the scheme: the unstable parcels move along θ surfaces in a neutral buoyant ascent.

The horizontal eddy flux term is normally neglected in upright convection when compared to the other large scale terms. In CSI, the contribution of this term is not yet clear. A scale analysis suggests that its magnitude can be comparable to the vertical eddy flux term. Assume that the slope of the transversal circulation is parallel to the θ surfaces, i.e.,

$$\frac{u'}{w'} = \frac{\partial \theta / \partial z}{\partial \theta / \partial x} = -\frac{N^2}{f V_z} \tag{6}$$

where N^2 is the Brünt-Väisälä frequency, f is the Coriolis parameter and V_z is the background horizontal wind shear.

The ratio between the horizontal and the vertical eddy flux terms can be scaled as:

$$\frac{\frac{\partial \left(\overline{\bar{\rho} u' m'}\right)}{\partial x}}{\frac{\partial \left(\overline{\bar{\rho} w' m'}\right)}{\partial z}} \sim \frac{\Delta z}{\Delta x} \frac{N^2}{f V_z} \tag{7}$$

Taking $\Delta z / \Delta x \sim 0.01$, $N^2 \sim 10^{-4} s^{-2}$, $f \sim 10^{-4} s^{-1}$, and $V_z \sim 10^{-2} s^{-1}$, the ratio in (7) is of order 1 in higher horizontal resolution models, or 0.1 in a coarser horizontal grid. So, this term is kept in the equations.

Using (6), (5) can be rewritten as:

$$\left(\frac{\partial \bar{m}}{\partial t}\right)_{SI} = -\frac{1}{\bar{\rho}} \left[\frac{\partial}{\partial x} \left(-\bar{\rho} \frac{N^2}{f V_z} \overline{w' m'} \right) + \frac{\partial}{\partial z} \left(\overline{\bar{\rho} w' m'} \right) \right] \tag{8}$$

By doing a coordinate transformation such that X is perpendicular and Z parallel to the θ surfaces, the eddy flux evaluated along the θ surface is

$$\left(\frac{\partial}{\partial Z}\right)_\theta \bar{\rho}\overline{w'm'} = -\frac{N^2}{fV_x}\frac{\partial}{\partial x}\bar{\rho}\overline{w'm'} + \frac{\partial}{\partial z}\bar{\rho}\overline{w'm'} \tag{9}$$

Assuming only small variations of N^2/fV_x, the l.h.s. of (9) can be substituted into (8),

$$\left(\frac{\partial \bar{m}}{\partial t}\right)_{SI} = -\frac{1}{\bar{\rho}}\frac{\partial}{\partial Z}\left(\bar{\rho}\overline{w'm'}\right) \tag{10}$$

where $\partial/\partial Z$ hereafter is assumed to mean the derivative along a θ surface. Note that in the limit of horizontal θ surfaces then $(X, Z) = (z, -x)$ whereas in the limit of vertical θ surfaces $(X, Z) = (x, z)$.

Essentially, the neutrality is achieved by mixing absolute momentum along the θ surfaces. The temperature field is not affected in this dry case, where potential temperature is conserved. However, in the moist version of the scheme, θ is no longer conserved, but θ_e, the equivalent potential temperature, is conserved. The temperature field would then be adjusted due to the condensation resulted from parcels ascending and becoming saturated.

The eddies can be parametrized in terms of mass fluxes, so the environment θ and m tendencies are expressed as:

$$\left(\frac{\partial \theta}{\partial t}\right)_{SI} = -\frac{1}{\bar{\rho}}\frac{\partial\left[M_u(\theta^p - \bar{\theta})\right]}{\partial Z} \tag{11}$$

$$\left(\frac{\partial m}{\partial t}\right)_{SI} = -\frac{1}{\bar{\rho}}\frac{\partial\left[M_u(m^p - \bar{m})\right]}{\partial Z} \tag{12}$$

where θ^p is the parcel potential temperature, m^p is the parcel absolute momentum, and M_u is the CSI mass flux. Since $\theta^p - \bar{\theta} \approx 0$, the adjustment of the environment to a neutral state to symmetric instability reduces to (12). Due to the two dimensional characteristic of the phenomenon, parcels conserve their absolute momentum. This turns into an advantage to the method because it is not necessary to make arbitrary estimates of the cloud absolute momentum; it is known exactly .

In CSI, the environment values are not the grid column values, as is the case for upright convection, but they are determined by the sloping path taken by the parcel. So,

the environment absolute momentum, which will be denoted by $\tilde{m}$, needs to be calculated. In an operational model, such as that at ECMWF, one has access at a given grid column not only to the temperature and wind but also to their gradients. We use this fact here to obtain a computationally efficient method to estimate $\tilde{x}$ and $\tilde{m}$.

Therefore $\tilde{m}$ is estimated from a first order approximation, using grid point values of m and $\frac{\partial m}{\partial x}$, i.e.

$$\tilde{m} = m(0,z) + \frac{\partial m(0,z)}{\partial x}\tilde{x} \tag{13}$$

where $\tilde{x}$ is the horizontal distance between the parcel and the grid point, which is at $x = 0$. The θ surface where the parcel is positioned can be written similarly as,

$$\tilde{\theta} = \theta^p = \theta(0,z) + \frac{\partial \theta(0,z)}{\partial x}\tilde{x} \tag{14}$$

where the neutral buoyant assumption has been used. Thus, the location of the parcel can be obtained by solving (14) for $\tilde{x}$,

$$\tilde{x} = \frac{\theta^p - \theta(0,z)}{\frac{\partial \theta(0,z)}{\partial x}} \tag{15}$$

The parcel path may span over the next grid columns, in this case an updated $\tilde{x}$ is estimated by taking the temperature and temperature gradient values from grid points nearest to the parcel.

$$\tilde{x}_{upd} = n\Delta x + \Delta\tilde{x} \tag{16}$$

where Δx is the horizontal grid spacing, n is the number of grid columns over which the parcel path spanned, and

$$\Delta\tilde{x} = \frac{\theta^p - \theta(n\Delta x,z)}{\frac{\partial \theta(n\Delta x,z)}{\partial x}} \tag{17}$$

The recalculation of $\tilde{x}$ by taking nearer temperature gradients, gives an improved $\tilde{m}$ estimate, and consequently, a better estimate of the cloud top level.

Assuming no convective instability, $\frac{\partial \theta}{\partial z} \geq 0$, the numerator in (15), $\theta^p - \theta$, will always be negative or zero. The direction that the θ surfaces slope will depend only on the sign of the horizontal temperature gradient, $\frac{\partial \theta}{\partial x}$, consequently, the sign of $\tilde{x}$ will give the same information. Therefore, the instability criterion (1) basically compares the slope of the θ surfaces and the slope of m surfaces through the correlation of $\tilde{x}$ and $\tilde{m}$, defined as the absolute momentum anomaly.

A constant, er, is added to $\hat{m}$ to account for uncertainties in its calculation, so that the instability criterion becomes $f(\hat{m}+er)\tilde{x} > 0$. The parameter er was arbitrarily chosen as $0.01m/s$, as it was noticed during the experiments that in its absence, the scheme kept working in regions of small instability, wasting computing time. On the other hand, the use of er one order of magnitude larger involved leaving some residual instability in the domain.

The instability criterion is tested from the lower levels upwards. The first grid level that satisfies this criterion is taken as the cloud base. The parcel will continue to rise until $\hat{m}$ changes sign, that is, $\hat{m} = 0$ has occurred, and the parcel loses its lifting force. The cloud top is taken as the highest level before $\hat{m}$ changes sign.

Equation (12) can be rewritten as:

$$\frac{\partial \tilde{m}}{\partial t} = -\frac{1}{\bar{\rho}} \frac{\partial \left[M_u (m^p - \tilde{m}) \right]}{\partial Z} \tag{18}$$

The adjustments $\Delta\tilde{m}$, calculated from (18), should be applied to the position of the parcel, however because the parcel at any level is rarely on a grid point, the tendencies are shared between the two nearest grid points, inversely proportional to their distances to the parcel. The velocity tendency $\Delta\tilde{v}$ is equal to $\Delta\tilde{m}$ as the adjustment is made at the location of the parcel.

It is interesting to note that from the definition of cloud base and cloud top, where $m^p - \tilde{m} = 0$, it follows that the restriction:

$$\int_B^T \frac{\partial \tilde{m}}{\partial t} dZ = -\int_B^T \frac{1}{\bar{\rho}} \frac{\partial \left[M_u (m^p - \tilde{m}) \right]}{\partial Z} dZ = 0 \tag{19}$$

is immediately satisfied. Here B and T stand for cloud base and cloud top, respectively.

By way of simplification only updraughts are considered within the cloud. The bulk equations for mass, heat and absolute momentum are:

$$\frac{\partial M_u}{\partial Z} = E - D \tag{20}$$

$$\frac{\partial (M_u m^p)}{\partial Z} = E\tilde{m} - Dm^p \tag{21}$$

where E and D are entrainment and detrainment of mass per unit length.

Turbulent entrainment can occur within the cloud layer. Detrainment occurs at the cloud top. Overshooting and subcloud fluxes are included in some sensitivity tests. Over-

shooting is considered by adding detrainment to one more level above the cloud top, and subcloud fluxes are distributed in more than one layer.

The cloud base mass flux is constrained by the CFL condition $M_u \leq \Delta z/\Delta t$. A value for $[M_u]_B$ chosen to be of the order of $0.5kgm^{-2}s^{-1}$ satisfies this condition for $\Delta z = 750m$ and $\Delta t = 750s$.

4 A Potential Vorticity view of the scheme

The instability criterion can be written in terms of the Ertel potential vorticity PV for a two-dimensional flow:

$$\bar{\rho}PV = \frac{\partial m}{\partial x}\frac{\partial \theta}{\partial z} - \frac{\partial m}{\partial z}\frac{\partial \theta}{\partial x} \tag{22}$$

Given that the presence of negative potential vorticity is one way to express the criteria for satisfying symmetric instability, it is interesting to analyze how this quantity can change following a parcel of air.

$$\frac{dPV}{dt} = f\frac{g}{\theta_0}\boldsymbol{\zeta}.\nabla Q + f\frac{g}{\theta_0}\boldsymbol{F}.\nabla\theta \tag{23}$$

On the r.h.s. of (23), the first term is due to frictional forces, $\boldsymbol{F}$, and the second due to diabatic processes, Q, such as radiative cooling, latent heat release or sensible heat. Note that for a moist atmosphere the instability criterion is in terms of the potential vorticity based on θ_e and that eq. (23) then has an extra term due to the angle between θ_e and θ. In the present study, where the large (resolved) scale atmosphere is assumed to be dry, two dimensional and frictionless, negative potential vorticity, or symmetric instability cannot be produced in a initially stable environment. However, if we take into account the scale separation, potential vorticity can be defined as the scalar product of large (resolved) scale absolute vorticity and large scale potential temperature, i.e. $\bar{\rho}PV = \bar{\boldsymbol{\zeta}}.\nabla\bar{\theta}$, where '-' denotes large scale area averaged variables.

An equation for the large-scale potential vorticity with the above assumptions can be obtained by applying the dot product of $\nabla\bar{\theta}$ with the large scale vorticity equation which is:

$$\frac{d\bar{\boldsymbol{\zeta}}}{dt} = \boldsymbol{\zeta}.\nabla\bar{\mathbf{u}} - \nabla\times\frac{1}{\bar{\rho}}\nabla.(\bar{\rho}\overline{\mathbf{u}'\mathbf{u}'}) \tag{24}$$

where on the r.h.s. of (24), the first term is the vortex tilting term, and the last term results from subgrid scale effects, such as turbulent transports of relative vorticity. Note the horizontal transports of eddies are kept. Assuming the fluid is incompressible the potential vorticity equation can be expressed in terms of large scale and subgrid scale variables, in the form

$$\frac{d}{dt}\left(\frac{\bar{\boldsymbol{\zeta}}.\nabla\bar{\theta}}{\bar{\rho}}\right) = -\frac{\bar{\boldsymbol{\zeta}}}{\bar{\rho}}.\nabla\left(\nabla.(\overline{\mathbf{u}'\theta'})\right) - \frac{1}{\bar{\rho}}\left[\nabla\times\frac{1}{\bar{\rho}}\nabla.(\bar{\rho}\overline{\mathbf{u}'\mathbf{u}'})\right].\nabla\bar{\theta} \tag{25}$$

Thus, in two dimensional atmosphere, with no resolved scale frictional or diabatic effects, potential vorticity can still be changed following the trajectory of a parcel due to subgrid scale frictional effects associated with turbulent mixing of heat and momentum.

In our idealised 2D model, where turbulent fluxes of heat are taken to be zero, this equation reduces to

$$\bar{\rho}\frac{dPV}{dt} = -\frac{\partial}{\partial x}\left[\frac{1}{\bar{\rho}}\frac{\partial(\bar{\rho}\overline{v'u'})}{\partial x} + \frac{1}{\bar{\rho}}\frac{\partial(\bar{\rho}\overline{v'w'})}{\partial z}\right]\frac{\partial\bar{\theta}}{\partial z} + \frac{\partial}{\partial z}\left[\frac{1}{\bar{\rho}}\frac{\partial(\bar{\rho}\overline{v'u'})}{\partial x} + \frac{1}{\bar{\rho}}\frac{\partial(\bar{\rho}\overline{v'w'})}{\partial z}\right]\frac{\partial\bar{\theta}}{\partial x} \tag{26}$$

Recalling eq. (5) for absolute momentum, where $m' = v'$, equation (26) can be expressed as:

$$\bar{\rho}\frac{dPV}{dt} = \frac{\partial}{\partial x}\left(\frac{\partial\bar{m}}{\partial t}\right)_{SI}\frac{\partial\bar{\theta}}{\partial z} - \frac{\partial}{\partial z}\left(\frac{\partial\bar{m}}{\partial t}\right)_{SI}\frac{\partial\bar{\theta}}{\partial x} \tag{27}$$

Thus,

$$\bar{\rho}\left(\frac{dPV}{dt}\right)_{SI} = \frac{\partial\dot{\bar{m}}}{\partial x}\frac{\partial\bar{\theta}}{\partial z} - \frac{\partial\dot{\bar{m}}}{\partial z}\frac{\partial\bar{\theta}}{\partial x} \tag{28}$$

where $\dot{\bar{m}} = \left(\frac{\partial m}{\partial t}\right)_{SI}$

The above expression gives the changes of potential vorticity of a parcel associated with the adjustments produced by the SI parametrization scheme. We will apply our SI scheme along θ-surfaces and in that case

$$\bar{\rho}PV = -\left(\frac{\partial m}{\partial z}\right)_{\theta}\frac{\partial\theta}{\partial x}. \tag{29}$$

$$\bar{\rho}\left(\frac{dPV}{dt}\right)_{SI} = -\left(\frac{\partial\dot{\bar{m}}}{\partial z}\right)_{\theta}\frac{\partial\theta}{\partial x}. \tag{30}$$

In order to test the SI mass flux parametrization scheme and to understand its adjustment process, the scheme is applied initially in section 5 to an unstable environment.

The scheme is assessed by the fraction of negative potential vorticity remaining in the domain. Further tests are applied in section 6 to the idealised flow, in which the initial conditions are stable to SI and a large-scale forcing is introduced so that a steady state can be examined where the forcing balances the parametrization tendencies.

5 Initially Unstable Flow

Two main groups of experiments were carried out: a single column cloud and a domain of grid columns.

5.1 single column cloud

A profile of absolute momentum along a θ surface containing symmetric instability is constructed. It is assumed that horizontal and vertical gradients of θ and m are positive. So, the first level where $\frac{\partial \tilde{m}}{\partial z} > 0$ occurs, or that $\hat{m} = m^p - \tilde{m} < 0$, is taken as the cloud base.

The adjustment is done by applying equation (18), taking $M_u = 0.5 kgm^{-2}s^{-1}$, $\Delta z = 750m$ and $\Delta t = 750s$. To be representative of the ECMWF forecast model an upstream difference scheme is used in discretizing (18), that becomes,

$$\Delta \tilde{m}(j) = -\frac{M_u \hat{m}(j+1) - M_u \hat{m}(j)}{\Delta z} \Delta t \tag{31}$$

where height $= j\Delta z$; $j = 1, 2, 3 \ldots$

The initial m profile along the θ surface shows a region in the centre of the domain where the wind increases with height. This profile contains instability in the layer between 5.25km and 12.75km, where the cloud base and cloud top are, respectively, considered to be located. The vertical wind shear is of the order of $7 \times 10^{-3} s^{-1}$ (Figure 2.a). The initial profiles of cloud mass flux, M_u, absolute momentum anomaly $\hat{m}$ and the product M_u is shown in Figure 2.b. In this experiment no turbulent entrainment or detrainment occurred in the cloud layer, so the mass flux was maintained constant there. Detrainment occurs at the cloud top, where M_u vanishes. The subcloud fluxes reaches zero in one layer just below the cloud base.

The instability is removed initially from upper levels downwards. The cloud top descends more rapidly than the cloud base. This results in decreasing the depth of the unstable layer. The wind shear is at the same time reduced. The adjusted m profiles, tend to stable rather than neutral profiles. The scheme also acts on regions outside the cloud layer, and hence the subcloud layer which is initially very stable, has its stability reduced. All instability in the column was eliminated in about 4hr or less.

Other tests were done to reproduce overshooting and subcloud fluxes. For example, to include the effects of cloud overshooting, the detrained mass is distributed over two layers above cloud top. The subcloud layer fluxes can be set to decrease to zero in one or two layers below the cloud base. The inclusion of these two processes produced, however, no significant changes to the adjusted profile. Very small differences can be noticed only near the cloud top and cloud base.

5.2 Whole cloud domain

5.2.1 initial conditions

An idealised absolute momentum, m, and potential temperature, θ, field is constructed in a two dimensional domain, in x and z directions. The temperature field consists of a basic state and a known perturbation function.

$$\theta = \bar{\theta}(x) + \theta'(x, z) \tag{32}$$

where $\bar{\theta}(x) = f\frac{\theta_0}{g}\bar{V}_z x + 300K$

The perturbation field comes from the arbitrary function:

$$\frac{\partial\theta'}{\partial z} = \frac{\theta_0}{g}\left(s_1 - s_0 \exp\left(\frac{-x^2}{a^2}\right)\sin\left(2\pi(z - dzc)\right)\right) \tag{33}$$

The value of the constants are:

$\frac{\theta_0}{g} = 30Km^{-1}s^2$, $s_1 = 0.119 \times 10^{-3}s^{-2}$, $s_0 = 0.575 \times 10^{-4}s^{-2}$, $\bar{V}_z = 0.75 \times 10^{-2}s^{-1}$, $f = 1.0 \times 10^{-4}s^{-1}$

Here a and dzc are the two parameters which are changed to produce different instability patches, and z is non-dimensional and varies between 0 and 1 from the bottom to the top boundary.

The temperature field can be constructed from: $\theta(x,z) = \bar{\theta}(x) + \int_0^z \frac{\partial \theta'}{\partial z} dz$. The thermal wind relation is used to calculate $\frac{\partial v'}{\partial z}$, from the prescribed perturbation. The meridional wind is also assumed to be: $v = \int_0^z (\bar{V}_x + \frac{\partial v'}{\partial z}) dz$. Finally, the absolute momentum is obtained from the meridional wind using: $m = v + fx$.

The original full $m-\theta$ field was constructed from eq.(33). It comprises 48 points in the horizontal, with a resolution of $\Delta x = 31.25km$, and 24 levels in vertical, with $\Delta z = 750m$. This field is supposed to represent a 'real' atmosphere. To simulate the coarse horizontal resolution of a large scale model, another field was constructed by taking a lesser number of grid columns equally spaced. This new field has lower horizontal resolution than the original one, and we refer to these data as "the analytical form". In the interior of this domain, θ lines slope more than the m lines and potential vorticity is negative. This is the region unstable to SI.

5.2.2 experiment characteristics

Several tests were carried out running the scheme over the whole domain.

The parameters $\tilde{x}$ and $\tilde{m}$ were estimated using eqs.(15) and (13) as would be done in an operational version of this scheme (note that in section 5.2.3 we use the known analytical values of $\tilde{x}$ and $\tilde{m}$ rather than these estimates). Different instability regions were constructed. Some sensitivity tests were made to include processes such as: entrainment, overshooting, and subcloud flux, and tests also for spatial resolution.

Entrainment is given by,

$$E_u(z) = \epsilon_u M_u(z) \tag{34}$$

where ϵ_u is the fractional turbulent entrainment rate, taken as, $\epsilon_u = 1. \times 10^{-4} m^{-1}$.

So, the entrainment rate in a layer $\Delta z = 750m$, can be written as,

$E(j) = 0.075 M_u(j-1)/\Delta z$

Detrainment occurs at cloud top. To check the sensitivity of the scheme to cloud top overshooting, detrainment is distributed over two layers, and taken as,

$D(top+1) = 0.75 M_u(top)/\Delta z$

$D(top+2) = 0.25 M_u(top)/\Delta z$

The cloud mass flux decreases to zero in the layer immediately below the cloud base. The sensitivity of the scheme to subcloud mass flux was also tested, with fluxes distributed

as;

$M_u\hat{m}(base-1) = 0.3M_u\hat{m}(base)$

$M_u\hat{m}(base-2) = 0.$

Experiments were done using 6 or 8 grid columns.

Due to the fact that in SI every parcel rises following a sloping θ surface, the parcels originating from a given pressure level in a (vertical) grid column, can be treated as essentially independent of those at other levels. This is unlike convection which, is represented by the ascent of a single parcel lifted from near the surface. A test was included, in which parcels from each pressure level in one grid column, unstable to SI, were separately lifted and the adjustments were applied simultaneously. This version of the scheme was called the 'multi base cloud' scheme.

The experiments can be listed as:

1a - 6 grid columns; entrainment, overshooting and subcloud fluxes included
1b - 8 grid columns;
2 - 6 grid columns; multi base cloud scheme

The horizontal resolution for the 6 grid column domain was $\Delta x = 281.25km$ and for the 8 grid column was $\Delta x = 187.5km$. The vertical resolution was kept as $\Delta z = 750m$.

The instability regions constructed for experiments 1 and 2 used the parameters: $a = 330km$ and $dzc = 0.20$. The initial field of $m - \theta$ surfaces and PV surfaces are shown in Figure 3.

Potential vorticity was integrated over the interior of the domain. The ratio between the area integrated initial total PV and the area integrated final total PV measures the conservation of PV by the scheme. The ratio between the initial integrated negative PV and the final integrated negative PV measures the fraction of the instability left in the domain by the scheme.

5.2.3 using exact $\tilde{x}$ and $\tilde{m}$ from analytical form

To evaluate the performance of the scheme without recourse to any estimation of $\tilde{x}$ and $\tilde{m}$, the position of the θ surface, and its environment absolute momentum, were taken

from the analytical formulae for the initial $m-\theta$ field, rather than from the estimates of eqs.(13) and (15). It was necessary, however, to apply a linear interpolation between neighbouring grid-point values to find the exact θ surface. The mass flux was kept constant in the cloud layer and experiment characteristics are otherwise as in experiment 1a.

The scheme removed 35% of the initial instability in 20 time steps, bringing the m surfaces almost parallel to the θ surfaces in the lower layers (Figure 4.a). This run showed that the scheme succeeds in removing or reducing the instability in a domain containing more than one grid column unstable to SI.

5.2.4 results obtained by estimation of $\tilde{x}$ and $\tilde{m}$

Initially, in the 6 grid column domain, the instability patch spanned over 2 grid columns, and in the 8 grid column domain, over 4 grid columns.

Figure 4.b-d show the adjusted $m-\theta$ and PV fields for the tests after $20\Delta t$ and Table 1 summarises some of these results. In table 1 column 2 is the average of negative PV for the initial state (i.e. it is the sum of PV over all grid-points at which $PV<0$ divided by the number of unstable grid-points). Column 3 gives the minimum value of PV found in the initial field. Negative PV, positive PV and the total PV are, respectively, summed in the domain for every time integration. The ratios between the initial and the adjusted sums of $-PV$, $+PV$ and total PV after $20\Delta t$ are shown in columns 4-6.

Apart from the very small changes at the cloud base and cloud top regions, the effects of considering cloud top overshooting and extended subcloud fluxes showed no significant changes or improvements to the scheme. Only for the cases of multi base cloud and for 8 grid columns, the exclusion of those effects resulted in slightly more efficient reduction of instability in the domain.

The inclusion of entrainment of mass removed slightly more instability from this domain. Due to the mixing with the environment, the cloud was less 'buoyant', the cloud tops occurred a little lower. The increase of total PV after 20 time steps was equal or less than 1%, indicating a relatively good conservation of total PV by the scheme. The relatively small decrease of $+PV$ is due to the fact that the initial $+PV$ is very large, and any small fraction is necessary to compensate the decrease of $-PV$ to conserve the total PV in the domain.

Table 1: Potential vorticity values for each experiment

Exp no	$-\overline{PV}_{init}$ (pvu)	PV_{min} (pvu)	$-PV$	$+PV$	PV_{tot}	Comment
1a	0.0479	-0.085	0.42	0.98	1.004	$20\Delta t$, 6 grid cols., entrainment overshooting and subcloud fluxes included
1b	0.0638	-0.127	0.16	0.95	1.008	$20\Delta t$, 8 grid cols.
2	0.0479	-0.085	0.04	0.98	1.010	$10\Delta t$, 6 grid cols., multi base cloud

The multi base cloud scheme reduces the instability in a much faster manner compared to the version of the scheme that each time step lifts only the lowest unstable parcels. This scheme reduced instability in a time scale of about 7-10hr, whereas the multi base cloud scheme reduced it in about 2-4hr. The latter time-scale agrees with that of the single column cloud tests.

In the 8 grid column test, the scheme adjusted the m surfaces along the θ surfaces more smoothly, in spite of the larger initial $-PV$ values. These results show that the spatial resolution may have an important effect on the performance of the scheme.

6 Forcing applied to an Initially Stable Flow

The presence of cumulus clouds affects the environment by cooling it through detrainment and warming it by cumulus induced subsidence. Vertical shear of horizontal wind, if present, is reduced through mixing processes between cloud and environment. On the other hand, the existence of the cloud itself is a result of processes such as advection, radiative cooling, or boundary layer fluxes. These are large scale processes which produce an environment suitable for developing cumulus clouds.

In some prognostic cumulus parametrization studies, observed data are taken as initial conditions, the model is run allowing a single cloud to develop and then decay when finally the environment is adjusted towards a state which is neutral to convection. The period of time until the cloud is eliminated is called the adjustment time. Precipitation and heating

distribution are compared with the observed data.

Assuming that the changes in the large scale processes occur on time scales much longer than the time scale of the cloud effects, it is reasonable to have the large scale forcing process applied during the time integration of the scheme. So, it is expected that clouds, or their parametrized effects, continuously counteract the action of the forcing in destabilising the environment. This is the basis of the Arakawa-Schubert convective scheme (Arakawa and Schubert 1974) in which an ensemble of clouds follow quasi equilibrium states with the large scale forcing. The final adjusted state is not necessarily towards a neutral state, but one with clouds in equilibrium with the large scale forcing. This is one of the advantages of including into the model a forcing term with a destabilising effect. In cloud parametrization studies, a steady state solution for the equations of motion can be sought. In the presence of forcing the adjustment time can also be determined. Another advantage of the use of forcing is the fact that it is a more realistic attempt to represent the atmosphere.

In the set of following experiments, large scale forcing is applied to the absolute momentum field, initially in the single column cloud, and afterwards in the whole cloud domain. The forcing is maintained constant during the time integrations, thus, when the scheme is switched on, the quasi-equilibrium state is also a quasi-steady state of $m - \theta$ field.

The absolute momentum adjustments produced by both processes should be approximately balanced in the quasi-steady state, i.e

$$\frac{\partial \bar{m}}{\partial t} = \left(\frac{\partial \bar{m}}{\partial t}\right)_{LS} + \left(\frac{\partial \bar{m}}{\partial t}\right)_{SI} \approx 0 \tag{35}$$

Similarly, the rate of change of negative or positive vorticity is approximately zero, that is,

$$\frac{\partial PV}{\partial t} = \left(\frac{\partial PV}{\partial t}\right)_{LS} + \left(\frac{\partial PV}{\partial t}\right)_{SI} \approx 0 \tag{36}$$

6.1 Single Column Cloud

The initial condition is defined by an absolute momentum profile of an environment which is symmetrically stable. Assuming the parcel trajectory is along the θ surface, this profile is represented by absolute momentum decreasing monotonically with height. In

this idealised model, absolute momentum decreases linearly, so the $m(z)$ profile is given by: $m(z) = m_o + \alpha z$, where m_o is the absolute momentum at the lowest model level, and α the shear of absolute momentum along the θ surface. A more negative value for α indicates an m profile less suitable for symmetric instability.

A simple time independent forcing is designed with a sinusoidal function in height and applied at the mid-levels of the profile. This forcing is given by:

$$\left(\frac{\partial \bar{m}}{\partial t}\right)_{LS} = \begin{cases} -A_c \sin \frac{2\pi(z-z_b)}{D_c} & \text{if } z_b < z < D_c + z_b \\ 0 & \text{otherwise} \end{cases} \tag{37}$$

where z_b is the height at cloud base, D_c is the depth of the cloud layer and A_c is a constant forcing amplitude. The advantage of this simple forcing is to keep the column integral absolute momentum constant.

The vertical resolution is taken as $\Delta z = 500m$ with 20 height levels, and the time step of integration, as $\Delta t = 500s$. The cloud mass flux, M_u, has to be smaller than $1kgm^{-2}s^{-1}$ to satisfy the CFL condition.

When the scheme is switched on, to counteract the destabilisation mechanism of the forcing, it is important to quantify the instability present in the column. Potential vorticity, measured by gradients along the θ-surface, indicates how much instability there is in the column, and how it evolves with time from equations (29) and (30).

A comparison between the magnitudes of the large scale forcing tendencies and the adjustments produced by the scheme, is from the ratio:

$$\frac{\left(\frac{\partial m}{\partial t}\right)_{LS}}{\left(\frac{\partial m}{\partial t}\right)_{SI}} = \frac{-A_c \sin \frac{2\pi(z-z_b)}{D_c}}{-\frac{1}{\bar{\rho}}\frac{\partial}{\partial z}[M_u(m^p - m)]} \tag{38}$$

Assuming no mass entrainment through the lateral boundaries of the cloud, the cloud mass flux and the parcel momentum is maintained constant in the cloud layer, so the relation (38) can be rewritten as

$$\frac{\left(\frac{\partial m}{\partial t}\right)_{LS}}{\left(\frac{\partial m}{\partial t}\right)_{SI}} = \frac{-A_c \sin \frac{2\pi(z-z_b)}{D_c}}{\frac{1}{\bar{\rho}} M_u \frac{\partial m}{\partial z}} \tag{39}$$

In the steady state, the scheme should be approximately balancing the large scale forcing, in this case, this relation should be ~ -1.

Thus, the steady state profile of absolute momentum can actually be predicted by taking (39) equal to -1, and integrating m from the cloud base z_b to a height z within the cloud layer, thus giving

$$m(z) = m^p + \frac{\rho A_c D_c}{M_u 2\pi}\left[1 - \cos\frac{2\pi(z - z_b)}{D_c}\right] \tag{40}$$

At the mid-layer height, $z_h = z_b + D_c/2$, we have the following relation

$$\frac{\Delta m}{\Delta z} = \frac{m(z_h) - m^p}{\frac{D_c}{2}} = \frac{2\rho A_c}{\pi M_u} \tag{41}$$

Whenever the forcing is present, $A_c > 0$, there will always exist a 'cloud' in the column, $\frac{\partial m}{\partial z} > 0$, however, this instability can be kept to a minimum, by having the ratio $\frac{\bar{\rho} A_c}{M_u}$ small. Equation (41) shows the magnitude of the unstable shear which remains in the layer in the steady state.

A set of single column cloud experiments were carried out. In these experiments the initial profile, the amplitude of the forcing and the cloud mass flux varied and the scheme was assessed under large scale forcing conditions.

6.1.1 Results

Figure 5.a,b,c show the results of the $6hr$ integration for the single column cloud with forcing and scheme on. The forcing has an amplitude, $A_c = 3.6ms^{-1}hr^{-1}$ applied at every time step. The cloud mass flux was fixed at $0.5kgm^{-2}s^{-1}$ giving a ratio of $\frac{\bar{\rho} A_c}{M_u} = 2.0ms^{-1}km^{-1}$, where density is taken as $1kgm^{-3}$. Figure 5.a shows the initial and adjusted m profiles along the θ surface. The initial shear was taken as $\alpha = -1.0ms^{-1}km^{-1}$.

At $t = 3.0hr$, the adjusted m profile has already reached a steady state. The steady 'cloud' has its base at $2500m$ and top at $7000m$, this is the layer in which the forcing is acting. The magnitude of the shear of the steady m profile is dictated by the forcing amplitude. At this time, the profile of the absolute momentum adjustments (Figure 5.b) due to the scheme is approximately balancing the absolute momentum tendencies produced by the forcing. It can be seen clearly, from the profile of the vertical gradient of absolute momentum along the θ surface (Figure 5.c), that at $t = 3.0hr$ a steady state has been established. The interpretation of the $\left(\frac{\partial m}{\partial z}\right)_\theta$ profile is that layers with negative gradients are stable to SI, while layers with positive gradients are unstable to SI. Positive values of

$\left(\frac{\partial m}{\partial x}\right)_\theta$ occurred in a shallow layer between $3000 - 4000m$. A very stable subcloud layer was produced as a result of the negative tendencies of the forcing applied immediately above the subcloud layer. The shear is kept of order $10^{-3}s^{-1}$, whereas in the absence of this parametrization scheme the shear is of the order of $10^{-2}s^{-1}$ after 3 hr.

The performance of the scheme can be evaluated by comparing the dotted curves with the solid curves in Figure 6. These curves show the maximum wind shear in the column and give a measure of the instability in the cloud layer and its progression in time. In the absence of the scheme, the forcing changes the initially stable shear to produce unstable shear which increases linearly with time. The rate of increase is controlled by the magnitude of the forcing. The presence of the counteracting effects of the parametrization scheme prevents the instability growing steadily. For the initial two hours, the scheme together with the forcing results in rather noisy curves (in time) of unstable shear. After these initial hours, both the scheme and the forcing tendencies start balancing each other as the variations in the curves become smaller. A steady state can also be identified in these curves as the unstable shear converges to a constant value given by the relation (41). The different solid curves show the dependence of the remaining unstable shear to the ratio $\frac{\bar{\rho}A_c}{M_u}$. An adjustment time scale of about $3.5hr$ can be assumed as after this time the variations are much smaller than they were initially.

Different initial profiles were tested: stable to SI ($\alpha = -1.0ms^{-1}km^{-1}$), strongly stable to SI ($\alpha = -2.0ms^{-1}km^{-1}$), and unstable to SI (figures not shown). After some time integration, the model reaches an equilibrium state which seems to be independent of the initial conditions.

6.2 Whole Cloud Domain

A two dimensional domain with absolute momentum and potential temperature fields was constructed using eq.(33). Some parameters were changed to produce an initial stable field. The modified parameters are: $a = 1000km$; $s_1 = 0.15 \times 10^{-3}s^{-2}$; $s_o = 0.57 \times 10^{-4}s^{-2}$ and $\bar{V}_s = 0.8 \times 10^{-2}s^{-1}$. The vertical resolution was taken as $\Delta z = 500m$ and the horizontal resolution was kept at $\Delta x = 281.25km$. The time step of integration was taken as $\Delta t = 500s$. The dimensions of the domain were $12.0km \times 2812.5km$, with 24 height levels and 11 grid columns. In this stable domain, absolute momentum surfaces slope

more than the potential temperature surfaces. A region of minimum potential vorticity is located in the centre (Figure 7).

The forcing is maintained constant during the time integrations. Its function is given as:

$$F_d(x,z) = A_d \exp\left(\frac{-(x-x_0)^2}{a_d^2}\right) \exp\left(\frac{-(z-z_0)^2}{b_d^2}\right) \sin\left(\frac{2\pi(z-z_0)}{D_d(x)}\right) \qquad (42)$$

where x_0 and z_0 is the coordinate point chosen to be the origin of the forcing function. The exponential dependence in x and z produces a damping in the amplitude of the forcing towards its borders. The simple sinusoidal function in z produces a change of sign of the forcing tendencies in the domain and maintains as constant the volume integral absolute momentum after every time integration. The depth of the forcing, $D_d(x)$ varies for different grid columns producing a population of clouds with different cloud top heights. The cloud base can also be different by tilting the forcing patch.

The multi-base cloud version of the scheme was used in the next set of experiments with the whole cloud domain and large scale forcing. These experiments consisted of varying the amplitude of the forcing and the magnitude of the cloud mass flux M_u and the shape of the forcing patch.

6.2.1 Results

A forcing of amplitude $A_d = 2.2ms^{-1}hr^{-1}$ and with its long axis sloping at a rate $1/225$ is applied on the right half of the domain (Figure 8). At $t = 12hr$ a large instability patch is fully developed and spans over three grid columns (Figure 9.a). Strong stable regions develop above and below the unstable patch. Taking $\dot{m}_F$ as the absolute momentum tendencies applied by the forcing, a negative potential vorticity region will be produced wherever $\frac{\partial \dot{m}_F}{\partial z} > 0$ and $\frac{\partial \dot{m}_F}{\partial x} < 0$, according to the forcing characteristics this results in an elongated and tilted patch.

When the parametrization scheme is included with a cloud mass flux, M_u, equal to $0.5kgm^{-2}s^{-1}$, the negative PV values are kept very small at $t = 12hr$, only the zero contour line shows (Figure 9.b). The regions of negative PV at this time are very similar to those at $t = 9hr$. When the forcing alone is modifying the absolute momentum field, θ surfaces slope much more than the m surfaces in the centre of the domain. In the experiments in which the scheme is switched on these surfaces are approximately parallel,

or closer to a neutral state, as Figure 9.b shows.

Experiments with different values of $\frac{\overline{\rho A_d}}{M_u}$ showed that a steady state is established in which the unstable shear has a magnitude given by this ratio in accordance with equation (41). Although less instability is produced with weak forcing, the region where it acts tends almost to neutrality with $m-\theta$ surfaces parallel and smoother. The overstabilisation above and below the cloud layer is minimised.

Figure 10.a-b show the rate of change of the summation of the potential vorticity in the interior of the domain. The total potential vorticity presents a good conservation during the whole time integration. The amount of symmetric instability reduced by the scheme can be assessed by comparing the curves from the experiment where the forcing acts alone with the curves from the experiment with the scheme counteracting the forcing. The total negative potential vorticity goes through cycles, this results from the competition between the forcing and the parametrization scheme adjustment. This curve suggests an adjustment time of about $8hr$.

A different forcing was constructed (figure not shown). The amplitude of the forcing was kept the same, but the tilt changed to $\sim -1/170$, oriented almost parallel to the θ surfaces. After 12hr of integration, this forcing produced smaller and weaker instability comparatively to the previous forcing. At $t = 12hr$, the potential vorticity field showed scattered and localised regions of negative PV, with reduced amplitude comparing with the case in which the forcing is acting alone. The momentum surfaces show more structure.

7 Concluding Remarks

The results given here indicate that a simple extension to the mass flux scheme for convection can operate to remove symmetric instability. The efficiency of the scheme was shown working under initially unstable conditions and initially stable conditions with forcing applied, either in a single column cloud or in the whole cloud domain. The rate at which the scheme effects a stabilisation of the atmosphere depends on the choice of M_u. The closure of the scheme by relating M_u to the resolved vertical velocity or moisture convergence has not been considered here.

The adjustment time for the single column cloud occurs in about 3 to $4hr$. The

whole cloud domain requires a longer adjustment time due to the interactive effects of the population of clouds.

The forcing represents the large-scale flow's tendency to increase the shear locally to produce symmetric instability. As this is equivalent to producing a sink of PV locally it can only occur via (unresolved) irreversible processes such as turbulence.

One conclusion from this study is that due to the sloping nature of parcel trajectories in SI there is a requirement to simultaneously perform adjustments due to the lifting of parcels from *each* vertical level in a grid column. This is different from convective instability which is taken as a vertical adjustment. This simultaneous lifting of several parcels in a given grid column we have called the 'multi-base cloud' scheme.

The scheme can also be easily extended for the full moist atmosphere. Questions such as whether current operational models need to include such a scheme have not been addressed herein.

Acknowledgments

The authors would like to acknowledge the help of Dr Martin Miller in formulating this scheme. Comments from Dr Thor Erik Nordeng have improved the paper.

References

[1] Bennetts, D. A. and Hoskins, B. J. 1979. Conditional Symmetric Instability - A possible explanation for frontal rainbands. *Quart. J. R. Meteor. Soc.*, **105**, p.945-962.

[2] Emanuel, K. A. 1983. The Lagrangian Parcel Dynamics of Moist Symmetric Instability.*J. Atmos. Sci.*, **40**, p.2368-2376.

[3] Emanuel, K. A. 1988. Observational Evidence of Slantwise Convective Adjustment. *Mon. Wea. Rev.*, **116**, p.1805-1816.

[4] Jones, S. C. and Thorpe, A. J. 1992. The three dimensional nature of "Symmetric Instability". *Quart. J. R. Meteor. Soc.*, **118**, p.227-258.

[5] Lindstrom, S. S. and Nordeng, T. E. 1992. Parametrized Slantwise Convection in a Numerical Model. *Mon. Wea. Rev.*, **120**, p.742-756.

[6] Nordeng, T. E. 1987. The Effect of Vertical and Slantwise Convection on the Simulation of Polar Lows. *Tellus*, **39A**, p.354-375.

[7] Sanders, F. and Bosart, L. F. 1985. Mesoscale structure in the megalopolitan snowstorm of 11-12 February 1983. *J. Atmos. Sci.*, **42**, p.1052-1061.

[8] Thorpe, A. J., Hoskins, B. J. and Innocentini, V. 1989. The parcel method in a baroclinic atmosphere. *J. Atmos. Sci.*, **40**, p.1274-1284.

[9] Thorpe, A. J. and Clough, S. A. 1991. Mesoscale dynamics of cold fronts - structure described by dropsoundings in FRONTS 87. *Quart. J. R. Meteor. Soc.*, **117**, p.903-941.

[10] Thorpe, A. J. and Rotunno, R. 1989. Nonlinear Aspects of Symmetric Instability. *J. Atmos. Sci.*, **46**, p.1285-1299.

[11] Tiedtke, M. 1989. A Comprehensive Mass Flux Scheme for Cumulus parameterization in Large Scale Models. *Mon. Wea. Rev.*, **117**, p.1779-1800.

Figure 1: Schematic cross section of an absolute momentum surface (solid line) and a potential temperature surface (dashed line). The parcel originating at the point (0,0) ascends along the theta surface up to T; $\tilde{x}$ is the horizontal displacement at the height $j\Delta z$, Δx and Δz are the horizontal and vertical grid spacings.

Figure 2: a) Absolute momentum (ms^{-1}) along the potential temperature surface (ms^{-1}). Initial (solid line) and adjusted (dashed line) profiles at $t = 4.2hr$. b) Initial cloud mass flux profile.

Figure 3: Initial potential temperature (dashed lines, contours: $5K$) and absolute momentum (solid lines, contours: $15ms^{-1}$) fields for Exp.1 and 2. Region of negative potential vorticity is shaded.

Figure 4: Adjusted potential temperature (dashed lines, contours: $5K$) and absolute momentum (solid lines, contours: $15ms^{-1}$) fields. Region of negative potential vorticity is shaded. a) Run using $\tilde{x}$ and $\tilde{m}$ from the initial dataset $t = 20\Delta t$. b) Exp.1a - $t = 20\Delta t$ c) Exp.1b - $t = 20\Delta t$ d) Exp.2 - $t = 10\Delta t$.

Figure 5: Experiment with forcing applied to a single column cloud. a) Profiles of absolute momentum along a potential temperature surface. The initial profile (solid line) is stable to SI so has negative vertical wind shear along θ surfaces; it is taken from a cyclonic region with positive horizontal gradient of temperature. The dotted line shows the m profile at $t = 6hr$ in the presence of the forcing but without the SI parametrization scheme acting. The dashed line shows the m profile for the case in which the scheme is included. b) Profiles of the forcing and scheme tendencies on the absolute momentum (ms^{-1}), for every $1.5hr$. c) Profiles of the vertical gradient of absolute momentum ($\times 10^{-2}s^{-1}$), for every $1.5hr$. $M_u = 0.5kgm^{-2}s^{-1}$, $A_c = 3.6ms^{-1}hr^{-1}$.

Figure 6: Rate of change of the unstable layer shear, $(\partial m/\partial Z)_{max}$, for different values of A_c and M_u applied to a single column cloud. Dashed and dotted lines lines refer to limiting cases when either no forcing or no scheme is acting. Solid line refer to experiments when both forcing and SI scheme are present. Units of A_c are given in $ms^{-1}hr^{-1}$ and M_u in $kgm^{-2}s^{-1}$.

Figure 7: Experiment with forcing applied to a whole cloud domain. Initial fields of potential temperature (dashed lines, contours: $5K$) and absolute momentum (solid lines, contours: $15ms^{-1}$). Region of *minimum* potential vorticity is shaded.

Figure 8: Absolute momentum forcing field. (Negative tendencies are dashed lines and positive tendencies are solid lines (contours:$0.08ms^{-1}$ per time-step).

Figure 9: Whole Cloud Domain Experiment. a) Forcing only ($A_d = 2.2ms^{-1}hr^{-1}$, tilt=$1/225$). $t = 12hr$. Adjusted potential temperature (dashed lines, contours: $5K$) and absolute momentum (solid lines, contours: $15ms^{-1}$) fields. b) Forcing and SI scheme. Adjusted potential temperature (dashed lines, contours: $5K$) and absolute momentum (solid lines, contours: $15ms^{-1}$) fields. Negative potential vorticity is shaded. ($M_u = 0.5kgm^{-2}s^{-1}$), $t = 12hr$.

Figure 10: Whole Cloud Domain Experiment. Rate of change of potential vorticity summed in the interior of domain. a)Forcing only. b)Forcing and SI scheme ($M_u = 0.5kgm^{-2}s^{-1}$). Total summation in solid, negative in dashed and positive in dotted lines.

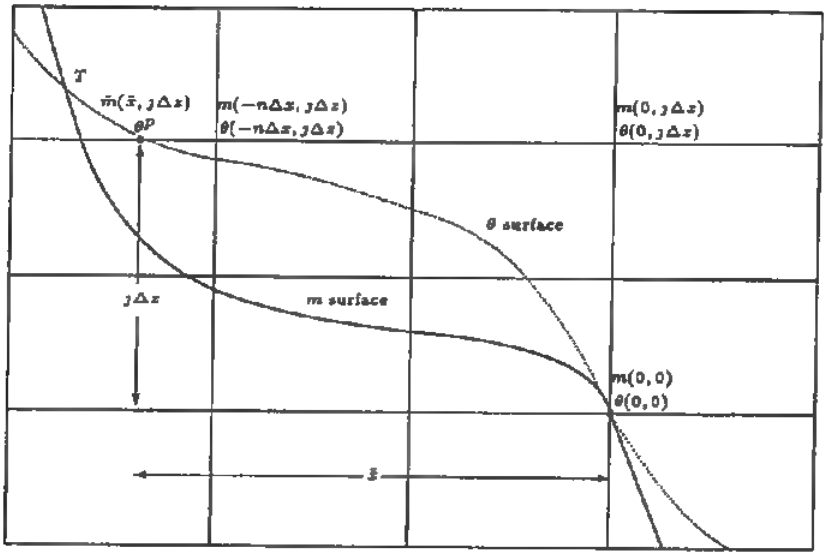

Figure 1: Schematic cross section of absolute momentum surface (solid line) and potential temperature surface (dotted line). The parcel originating at the point (0,0) ascends along the θ surface up to T. $\tilde{x}$ is the horizontal displacement at the height $j\Delta z$. Δx and Δz are the horizontal and vertical grid spacings.

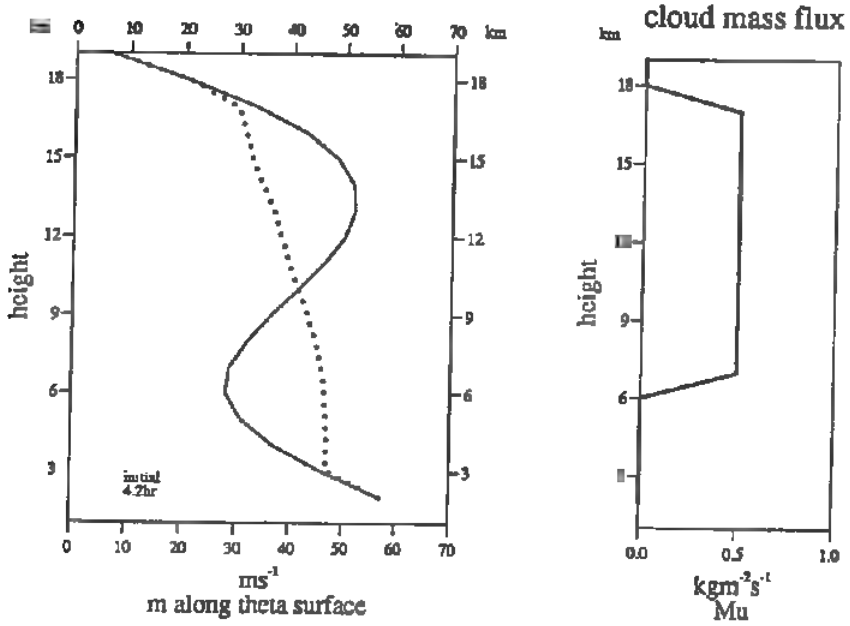

Fig 2 a b

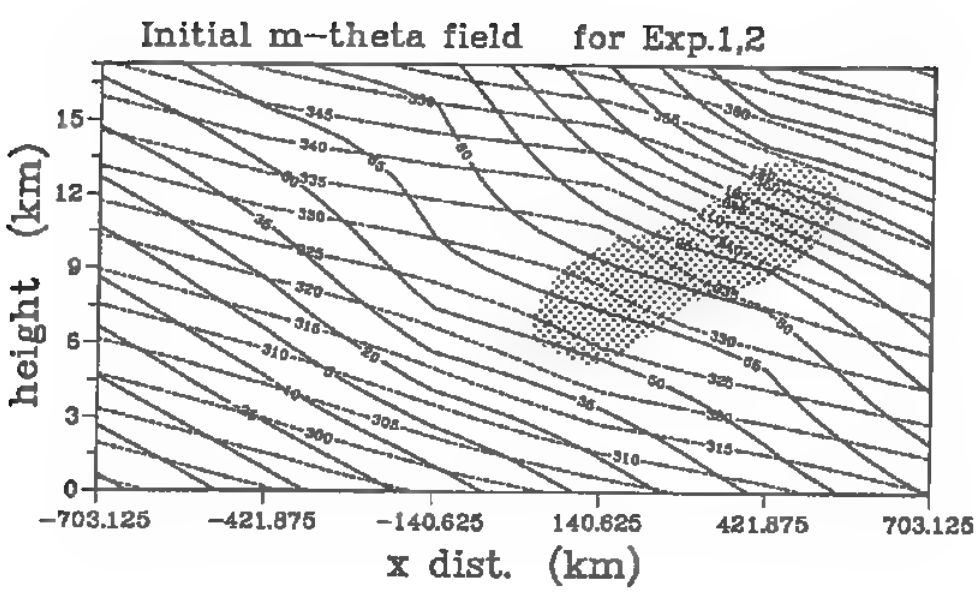
Initial m-theta field for Exp.1,2
height (km)
15
12
9
6
3
0
−703.125
−421.875
−140.625
140.625
421.875
703.125
x dist. (km)

Fig. 3

a

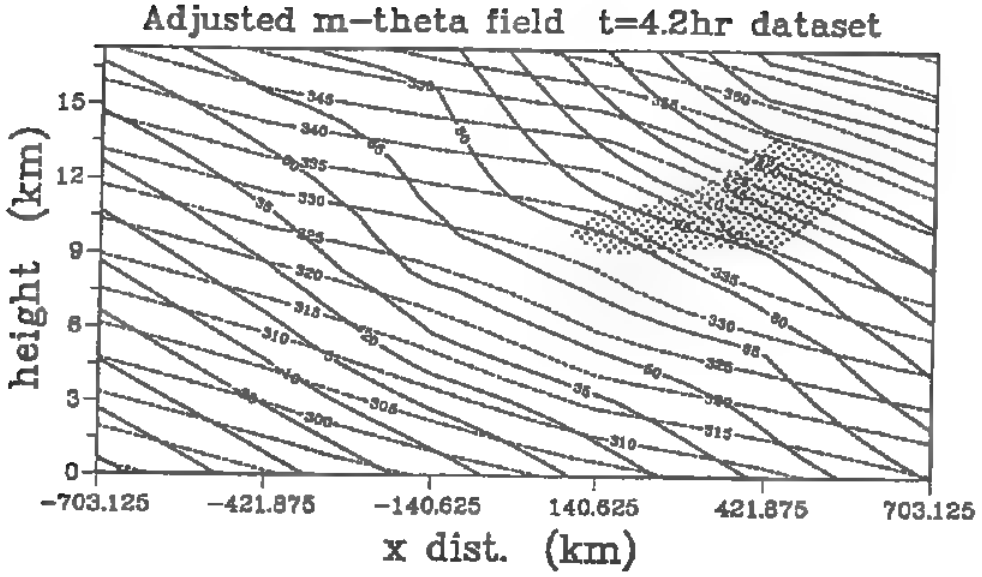
Adjusted m-theta field t=4.2hr dataset
height (km)
0
3
6
9
12
15
-703.125
-421.875
-140.625
140.625
421.875
703.125
x dist. (km)

b

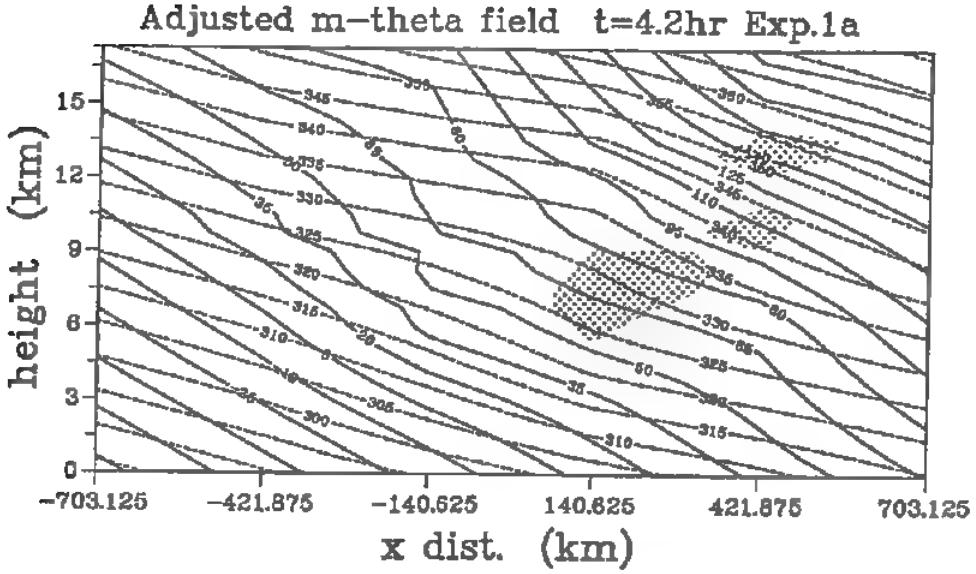
Adjusted m-theta field t=4.2hr Exp.1a
height (km)
0
3
6
9
12
15
-703.125
-421.875
-140.625
140.625
421.875
703.125
x dist. (km)

c

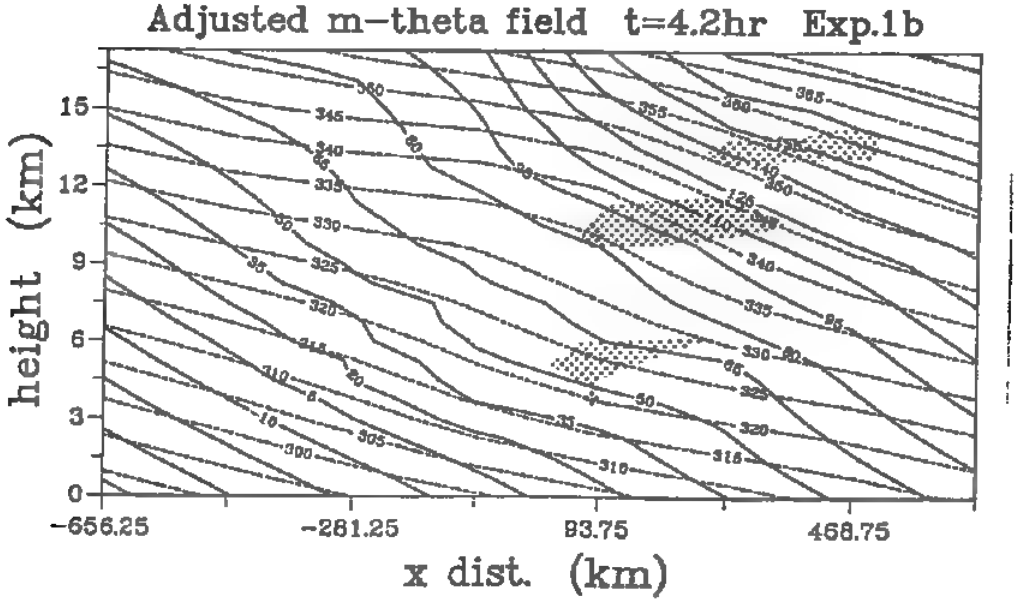
Adjusted m-theta field t=4.2hr Exp.1b
height (km)
0
3
6
9
12
15
-656.25
-281.25
93.75
468.75
x dist. (km)

Fig.4

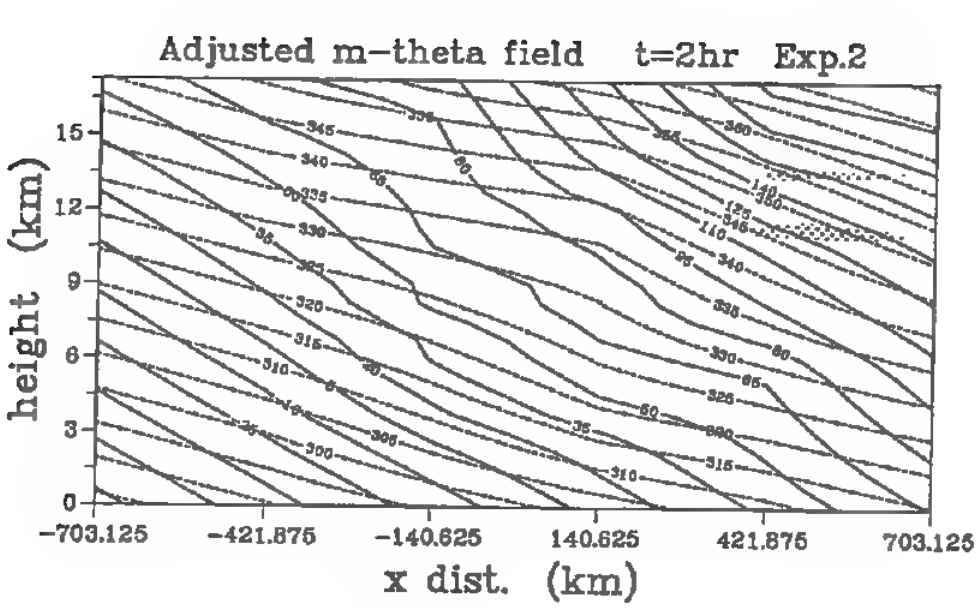
Adjusted m-theta field t=2hr Exp.2
height (km)
15
12
9
6
3
0
-703.125
-421.875
-140.625
140.625
421.875
703.125
x dist. (km)

Fig 4 d

a

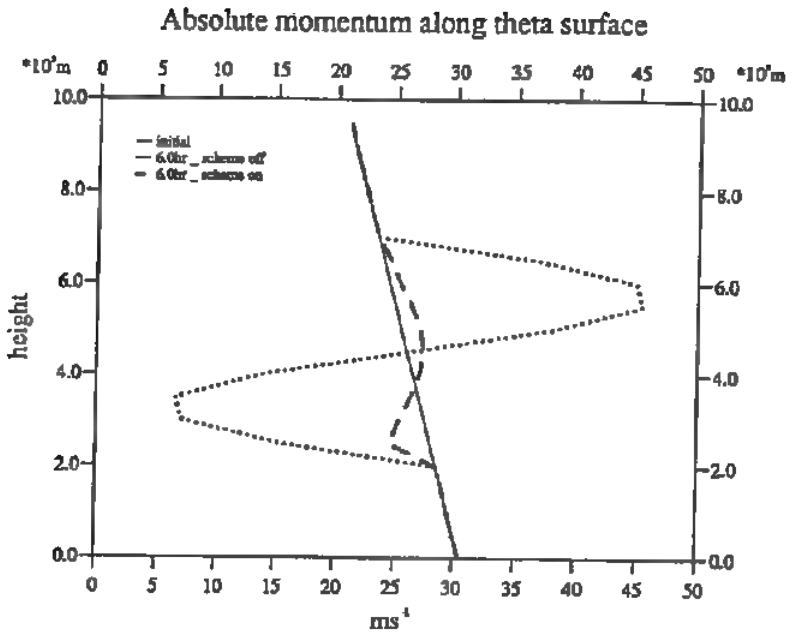
Absolute momentum along theta surface
*10³m
height
ms⁻¹

b

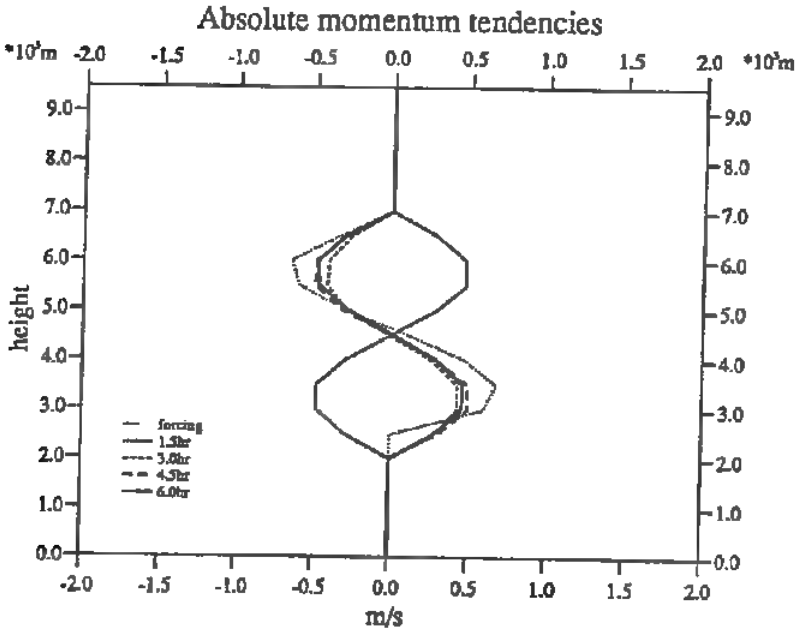
Absolute momentum tendencies
*10³m
height
forcing
1.5hr
3.0hr
4.5hr
6.0hr
m/s

c

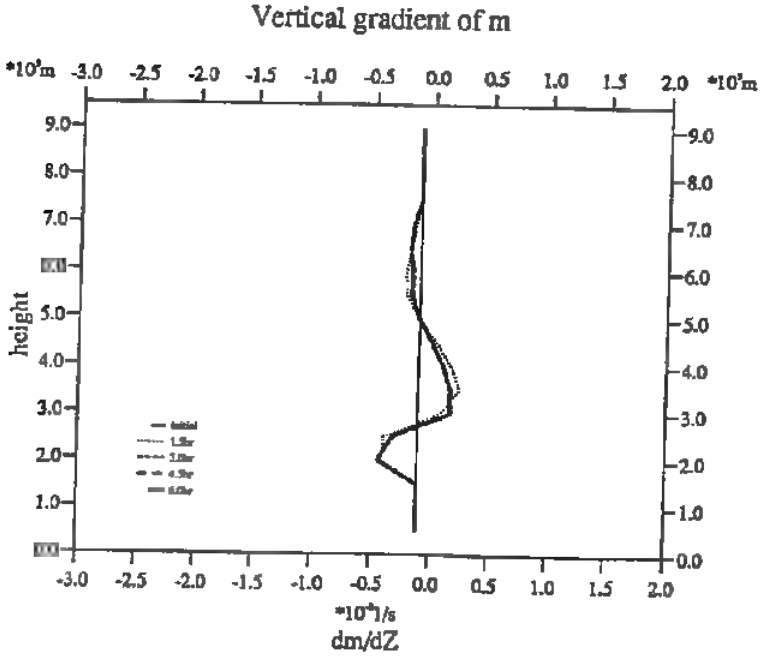
Vertical gradient of m
*10³m
height
*10⁻³l/s
dm/dZ

Fig 5

Fig 6

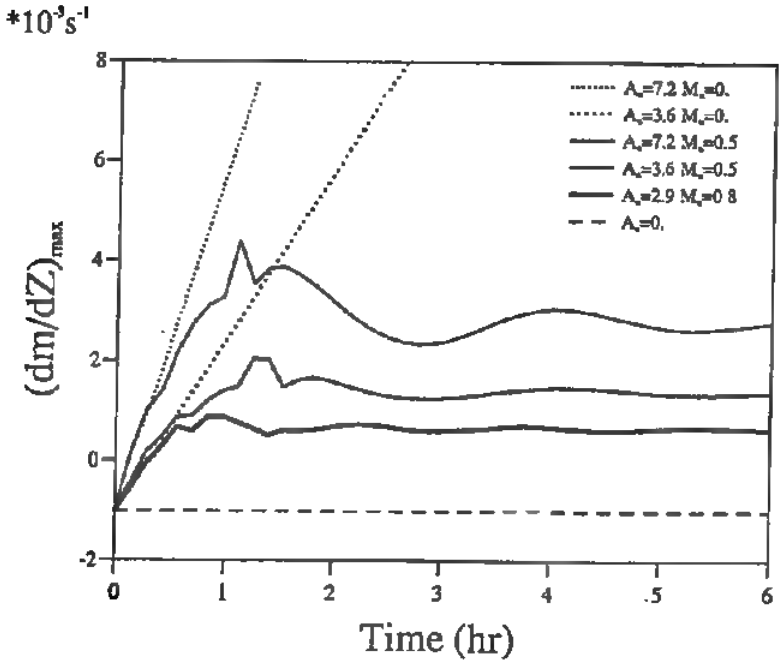

Fig.7

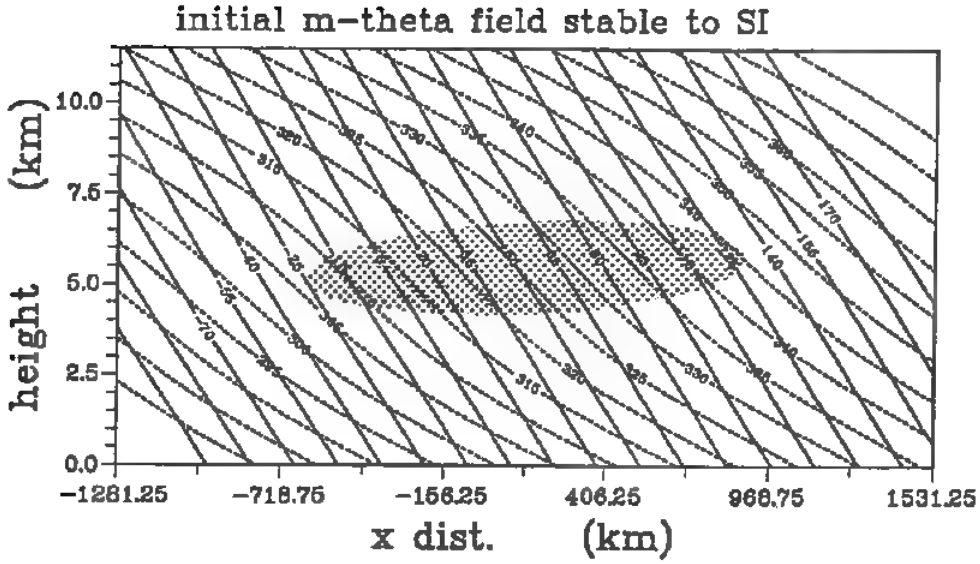

Fig.8

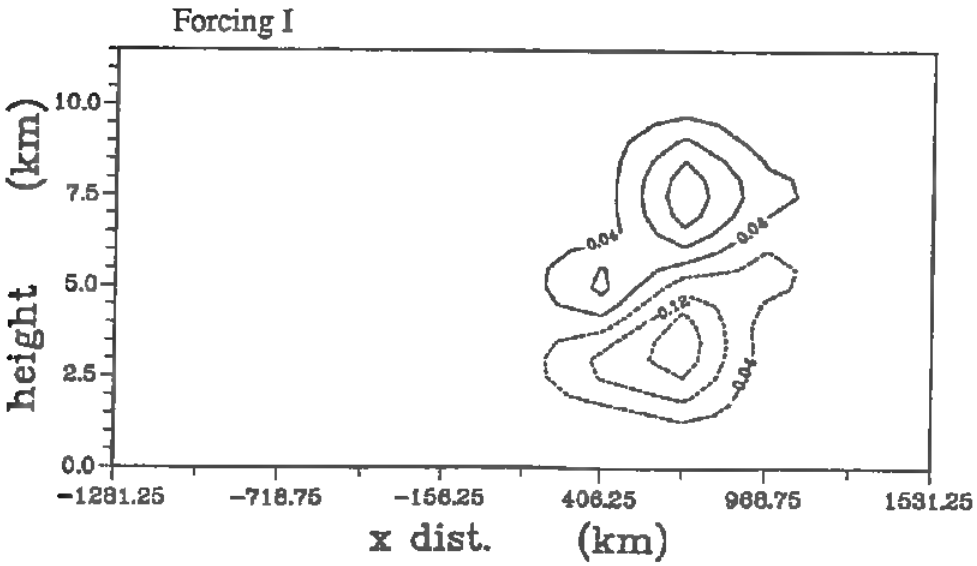

a

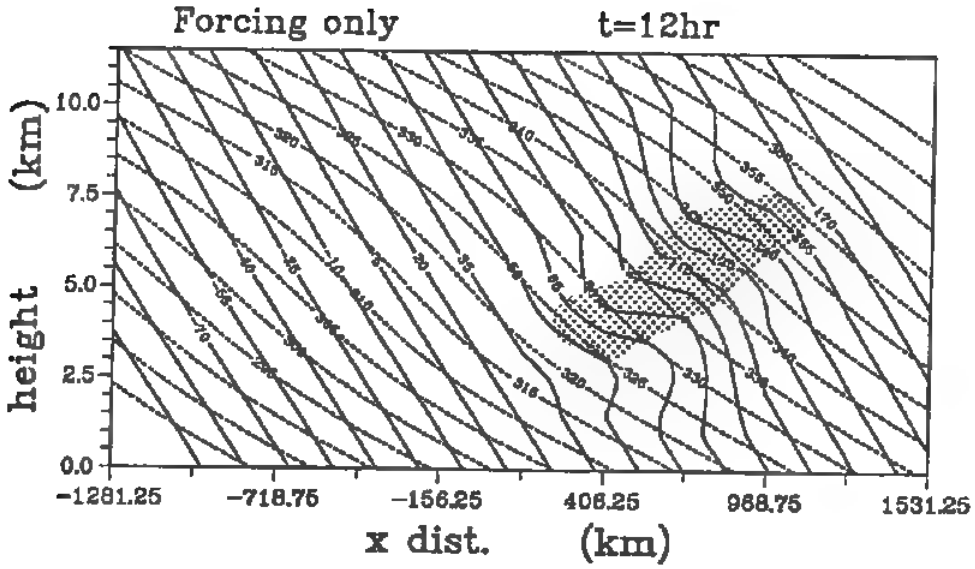
Forcing only
t=12hr
height (km)
10.0
7.5
5.0
2.5
0.0
-1281.25
-718.75
-156.25
406.25
968.75
1531.25
x dist. (km)

b

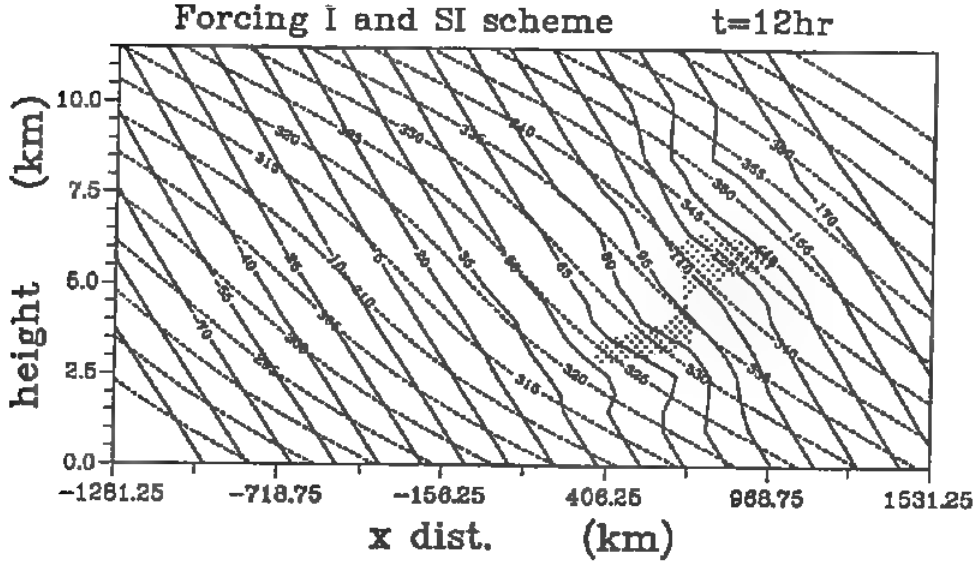
Forcing I and SI scheme
t=12hr
height (km)
10.0
7.5
5.0
2.5
0.0
-1281.25
-718.75
-156.25
406.25
968.75
1531.25
x dist. (km)

Fig 9

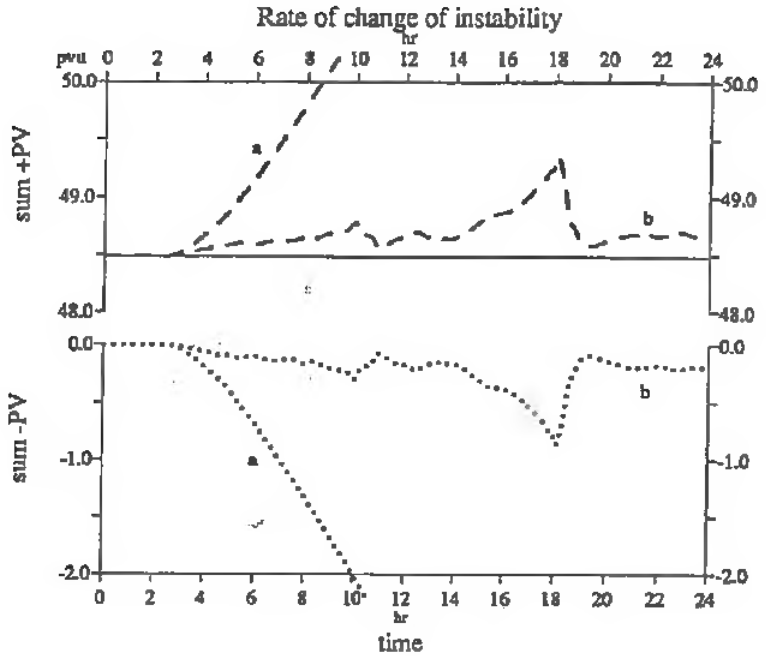
Rate of change of instability
pvu
hr
0
2
4
6
8
10
12
14
16
18
20
22
24
50.0
49.0
48.0
sum +PV
a
b
0.0
-1.0
-2.0
sum -PV
time

Fig 10

CURRENT JCMM INTERNAL REPORTS

This series of JCMM Internal Reports, initiated in 1993, contains unpublished reports and also versions of articles submitted for publication. The complete set of Internal Reports is available from the National Meteorological Library on loan, if required.

1. **Research Strategy and Programme.**
   K A Browning et al
   January 1993

2. **The GEWEX Cloud System Study (GCSS).**
   GEWEX Cloud System Science Team
   January 1993

3. **Evolution of a mesoscale upper tropospheric vorticity maximum and comma cloud from a cloud-free two-dimensional potential vorticity anomaly.**
   K A Browning
   January 1993

4. **The Global Energy and Water Cycle**
   K A Browning
   July 1993

5. **Structure of a midlatitude cyclone before occlusion.**
   K A Browning and N Roberts
   July 1993

6. **Developments in Systems and Tools for Weather Forecasting.**
   K A Browning and G Szejwach
   July 1993

7. **Diagnostic study of a narrow cold frontal rainband and severe winds associated with a stratospheric intrusion.**
   K A Browning and R Reynolds
   August 1993

8. **Survey of perceived priority issues in the parametrizations of cloud-related processes in GCMs.**
   K A Browning
   September 1993

9. **The Effect of Rain on Longwave Radiation.**
   I Dharssi
   September 1993

10. **Cloud Microphysical Processes - A Description of the Parametrization used in the Large Eddy Model.**
    H Swann
    October 1993

11. **An Appreciation of the Meteorological Research of Ernst Kleinschmidt.**
A J Thorpe
May 1992

12. **Potential Vorticity of Flow Along the Alps.**
A J Thorpe, H Volkert and Dietrich Heimann
August 1992

13. **The Representation of Fronts.**
A J Thorpe
January 1993

14. **A Parametrization Scheme for Symmetric Instability: Tests for an Idealised Flow.**
C S Chan and A J Thorpe
February 1993

Met Office Joint Centre for Mesoscale Meteorology Department of Meteorology
University of Reading PO Box 243 Reading RG6 6BB United Kingdom
Tel: +44 (0)118 931 8425 Fax: +44 (0)118 931 8791
www.metoffice.com